INTERNATIONAL JOURNAL OF CIRCUIT THEORY AND APPLICATIONS
Int. J. Circ. Theor. Appl. (2009)
Published online in Wiley InterScience (www.interscience.wiley.com). DOI: XX.XXXX/cta.XXX

Modeling of Switching Frequency Instabilities in Buck-Based DC-AC H-Bridge Inverters

Abdelali El Aroudi[1,*,†], Enric Rodriguez[2], Mohamed Orabi[3] and Eduard Alarcón[2]

[1] *Departament d'Enginyeria Electrònica, Elèctrica i Automàtica (DEEEA) Universitat Rovira i Virgili, Tarragona, Spain,*
[2] *Departament d'Enginyeria Electrònica, Universitat Politècnica de Catalunya, Barcelona, Spain*
[3] *APEARC, South Valley University Aswan, Egypt*

SUMMARY

In this paper, the dynamical behavior of a full bridge DC-AC buck inverter controlled by fixed frequency and PWM is studied. After showing that the system can undergo both period-doubling and Neimark-Sacker bifurcation at the fast scale (switching period) by using the exact switching model, an exact solution discrete-time model able to predict both instability phenomena is derived. The model is obtained without making the quasi-static approximation and it can be used to obtain the useful operation region in the multidimensional design parameter space from time domain simulations in a very fast and accurate manner. Based on the study of the system, some design guidelines are provided. Copyright © 2009 John Wiley & Sons, Ltd.

KEY WORDS: Stability Analysis, Discrete Time Model, Bifurcations, DC-AC buck, Inverters, H-bridge

1. Introduction

Obtaining accurate mathematical models for switching power electronics circuits is a traditional challenge for the power electronics engineers [1]. Many of the reported analysis on power electronics circuits are based on averaging technique. However, averaging is only an approximated procedure to obtain the low frequency behavior of the actual switching system. Recent findings show that elementary switching circuits like DC-DC buck converter under PWM control are prone to subharmonic oscillations that can not be understood and predicted by using the averaged model. During the two last decades, a large variety of complex nonlinear behaviors have been shown to be possible, firstly, for simple power electronics circuits. An extensive literature is devoted to nonlinear dynamics arising in elementary DC-DC converters [30]-[33]. Later, and realizing the practical importance of AC-DC converters and motivated by

*Correspondence to: Abdelali El Aroudi, Departament d'Enginyeria Electrónica, Eléctrica i Automática (DEEEA)
Universitat Rovira i Virgili, Tarragona, Spain.
†E-mail: abdelali.elaroudi@urv.cat

Received Oct. 5th 2008
Revised XX YY ZZZZ
Accepted June 13rd 2009

the need to clarify some of the nonlinear behaviors that the system may undergo, a series of studies have been carried out for these nonlinear time-varying systems [**?**]-[10]. More recent results related to these topics can be found in the works reported in [28]-[32], where some studies about the existence of bifurcations and chaotic behavior in DC-DC converters and AC-DC power factor corrector circuits are presented. These studies allowed a deeper understanding of their fundamental properties and dynamic behavior. However, less research activity has been carried out for DC-AC inverters which are largely used in renewable energy systems applications like photovoltaic (PV) energy processing [15].

A PV array can generate only direct current (DC) electricity. This DC electricity can be converted to alternating current (AC) with relative ease and efficiency through the use of an inverter. An inverter is a device that takes a DC input voltage (*e.g.* from a battery bank charged from a renewable energy source like a PV array, a fuel cell or supply grid in UPS applications) and produces a sinusoidal AC output voltage under a certain control scheme. There exist many inverter topologies that can be designed depending on the situation and the requirements. They need to be designed to handle the requirements of an energy-hungry household yet remain efficient during periods of low demand and stable under parameter variations. The waveform output choices for DC-AC inverters include pure sine wave, square wave, stepped wave, and triangular wave. Pure sine wave is the best waveform, as it is the shape of an ideal AC electrical signal from the power line. Due to their advantages, sine wave inverter have received research efforts bout developing new topologies or implementing sophisticated control schemes [16]. The main drawback of this kind of systems is their inherent switching nonlinearity.

Being a switched nonlinear and time-varying switching system, a DC-AC power electronic inverter is prone to instability as parameters are varied. In [17], [18] and [19] an effort was made to model the nonlinear behavior of a DC-AC chopper by considering a purely resistive load and under current mode control. The authors demonstrated, through mathematical analysis of a simple discrete-time model obtained by assuming the reference current to be constant and numerical simulations, that the system can undergo period-doubling bifurcation when some suitable design parameters are tuned in some ranges. Later, the authors showed in other works that these bifurcations can be categorized within the class of border collision bifurcations [20]. In many reported works, even if a capacitive filter is considered at the output and the system considered is two-dimensional, the authors make the quasi-static approximation to derive the discrete-time model by considering the reference voltage to be constant, which results in a model identical to that of a DC-DC buck regulator. However, the presence of a sinusoidal reference make inverters with dynamical characteristics very different to those of DC-DC converters and this is similar to what can occur in AC-DC power factor correctors [8]-[11]. These time-varying systems are more complex in the sense that their dynamics are characterized naturally by two different periods and therefore by two different time scales. The impact of this coexistence of dynamics is particularly relevant if the ratio of the switching frequency to the reference frequency is low.

In this paper we will carry out a careful modeling of a DC-AC full bridge buck inverter being the approach similar to other switching time-variant circuits like AC-DC and AC-AC converters. We will deal with the reference voltage as a sinusoidal signal and no quasi-static approximation will be assumed. A dynamic controller in the form of a low pass filter for the outer voltage loop is considered and its dynamics are taken into account in the model. The purpose of this compensator is to provide proportional gain and to reject high frequency ripple.

It is obtained that the map is time-varying in the discrete-time domain and that its steady state is a periodic orbit, not a fixed point like it is traditionally assumed. The aim is to present an accurate model to describe the dynamics of the system, to predict instabilities that can occur and to use this model to derive some stability boundaries in an appropriate design parameter space. The remainder of the paper is organized as follows. Section II will deal with the system description and modeling. Both the switched and the averaged models are derived for the system. By using the averaged model, some analytical expressions giving the stability boundaries in suitable design parameter spaces are obtained. Section III shows numerical simulations from the switched circuit-based model revealing interesting phenomena that the system can exhibit. Different instability phenomena are presented. Then, in Section IV, the discrete-time model is derived and it is used to obtain some numerical simulations of the system. Design-Oriented stability boundaries are shown in Section V. Finally, some conclusions are given in the last section.

2. System Description

2.1. Modeling of the power stage

The schematic diagram of a DC-AC buck-based inverter is shown in Fig. 1. The activation of the switches S_i is carried out as follows: S_1 and S_4 are driven synchronously while S_2 and S_3 are driven in a complimentary manner to S_1 and S_4 respectively. The output voltage is sensed and the voltage error represented by the difference voltage $v_{\text{ref}} - v_{\text{o}}$ is processed by means of a voltage controller in the form of a low-pass filter. The output v_{con} of this controller is connected to the non-inverting input of the comparator whereas a sawtooth ramp generator is applied to the inverting input, in such a way that in steady state the switches S_1 and S_4 are activated each switching cycle while they are turned OFF whenever the ramp voltage $v_{\text{ramp}}(t)$ crosses the control signal $v_{con}(t)$.

The circuit is designed in order to provide periodic waveforms of state variables. There are two periods that characterize the dynamics of the system in steady state: the switching period T_s and the reference voltage period T_r. The stationary periodic attractor is settled therefore into a two-dimensional torus characterized by two periods: the switching period and the reference period. The system of state equations for the power stage during first phase (S_1 and S_4 closed) is given by:

$$\begin{aligned} \frac{dv_C}{dt} &= -\frac{v_C}{RC} + \frac{i_L}{C} \\ \frac{di_L}{dt} &= \frac{V_{\text{in}} - v_C}{L} \end{aligned} \tag{1}$$

whereas during the second interval (S_1 and S_4 open), the following equations for the state variables are obtained:

$$\begin{aligned} \frac{dv_C}{dt} &= -\frac{v_C}{RC} + \frac{i_L}{C} \\ \frac{di_L}{dt} &= -\frac{V_{\text{in}} + v_C}{L} \end{aligned} \tag{2}$$

where L is the inductance of the inductor, C is the capacitance of the capacitor, R is the load

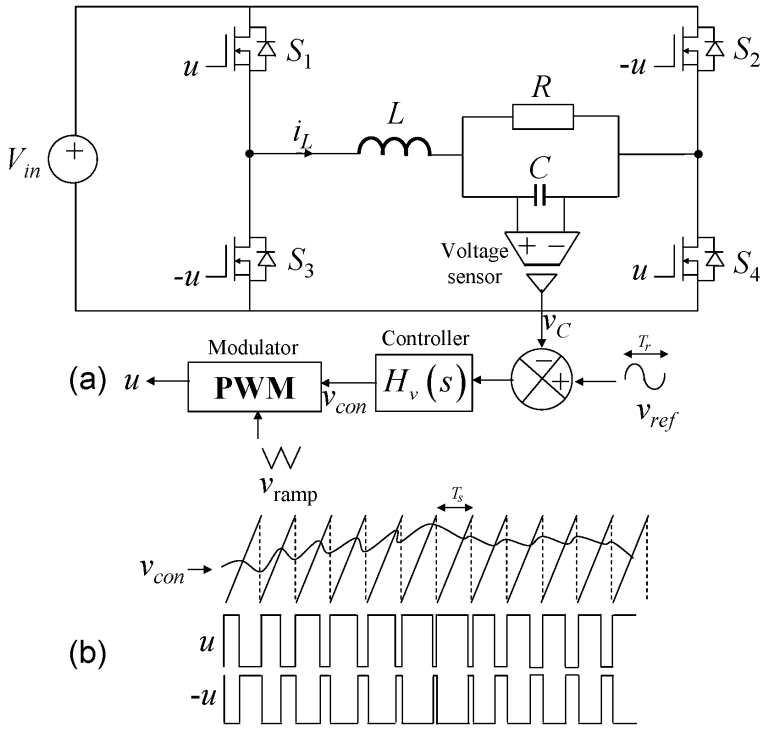

Figure 1. DC-AC H-bridge buck-based inverter under fixed frequency voltage-mode control. (a) Circuit diagram, (b) representative signal of the PWM modulator.

resistance, v_C is the output capacitor voltage, i_L is the inductor current and V_{in} is the input voltage.

2.2. Modeling of the output voltage controller

With the purpose that the output voltage v_C tracks a desired sinusoidal reference $v_{\text{ref}} = V_r \sin(\omega_r t)$, an outer voltage loop controller in the form of a dominant pole (low pass-filter) is used. The pole of the controller $f_v = 1/\tau_v$ is a design parameter that should be adjusted together with other parameters in such a way that the ripple in the feedback control voltage is small and that the crossover frequency ω_c remain much smaller than the switching frequency. In the frequency domain, the small signal transfer function of this controller can be written in the following form:

$$H_v(s) := \frac{\tilde{v}_{con}(s)}{\tilde{v}_{\text{error}}(s)} = \frac{k_v}{1 + s\tau_v} \tag{3}$$

where $v_{\text{error}} = v_{\text{ref}} - v_{\text{o}}$ and k_v is the filter DC gain. This dynamic controller defines a third state variable for the system whose dynamic behavior is given by:

$$\frac{dv_{con}}{dt} = \frac{1}{\tau_v}\left(-v_{con} + k_v\left(v_{\text{ref}} - v_C\right)\right) \tag{4}$$

2.3. Compact form expression of the exact switched model

The switched model of the system can be written in the following form:

$$\begin{aligned} \dot{\mathbf{x}} &= \mathbf{A}\mathbf{x} + \mathbf{B}_1(t) \qquad \text{during phase 1} \\ \dot{\mathbf{x}} &= \mathbf{A}\mathbf{x} + \mathbf{B}_2(t) \qquad \text{during phase 2} \end{aligned} \tag{5}$$

where $\mathbf{x} \in \mathbb{R}^3$ is the vector of state variables whose entries are the capacitor voltage v_C, inductor current i_L, and the control voltage v_{con}. $\mathbf{A} \in \mathbb{R}^{3\times 3}$ and $\mathbf{B} \in \mathbb{R}^3$ are the system matrices and vectors given by:

$$\mathbf{A} = \begin{pmatrix} -\frac{1}{RC} & \frac{1}{C} & 0 \\ -\frac{1}{L} & 0 & 0 \\ -\frac{k_v}{\tau_v} & 0 & -\frac{1}{\tau_v} \end{pmatrix}, \mathbf{B}_1(t) = \begin{pmatrix} 0 \\ \frac{1}{L}V_{\text{in}} \\ \frac{k_v}{\tau_v}V_r \sin(\omega_r t) \end{pmatrix}, \mathbf{B}_2(t) = \begin{pmatrix} 0 \\ -\frac{1}{L}V_{\text{in}} \\ \frac{k_v}{\tau_v}V_r \sin(\omega_r t) \end{pmatrix} \tag{6}$$

A compact form expression for the switched model of the system can be expressed by the following nonlinear time-varying model:

$$\dot{\mathbf{x}} = \mathbf{A}\mathbf{x} + (\mathbf{B}_1(t) - \mathbf{B}_2(t))u(t) + \mathbf{B}_2(t) \tag{7}$$

Taking into account the switching decision described above and that the control signal can take values in the set {0,1}, the switched model of the system can be written as:

$$\dot{\mathbf{x}} = \mathbf{A}\mathbf{x} + (\mathbf{B}_1(t) - \mathbf{B}_2(t)) \left[\frac{1}{2} + \frac{\text{sign}(v_{con}(t) - v_{\text{ramp}}(t))}{2}\right] + \mathbf{B}_2(t) \tag{8}$$

where 'sign' stands for the signum function that describes the switching action when v_{con} and v_{ramp} intersect. Unlike the DC-DC converter case, the duty cycle is time-varying from cycle to cycle even in steady state operation. The duty cycle corresponding to a switching period can be obtained by solving the equation resulting from the crossing of the ramp signal with the control voltage $v_{con}(t)$ in this period. In this paper, we consider a ramp signal with offset value V_l, maximum value V_u and positive slope. In this case, the switching condition during one period can be written as:

$$\sigma(\mathbf{x}, t) := v_{con}(t) - V_l - (V_u - V_l)\frac{t}{T} = 0 \tag{9}$$

If Eq. (9) is not feasible and $v_{con} > V_u$ then d is set to 1 whereas it is set to 0 if $v_{con} < V_l$. Representative simulations to be shown in the next section consider the above described switched model.

2.4. Small signal averaged model

Eq. 8 represents a switched discontinuous vector filed due to the presence of the discontinuous driving signal $u(t)$. A traditional approach for studying the stability and performances and

characterizing its dynamical behavior is by means of numerically solving this discontinuous equation and simulating the system behavior for different value of parameters and under different operating points. This method has the disadvantage of being computationally intensive. An alternative approach is by averaging the system equation over a switching period to remove the discontinuity due to the switching action. Further simplification is obtained by considering the reference signal to be constant and replacing it by its RMS value. In this way, the small signal transfer function for the system can be obtained and conclusions about its slow scale dynamical behavior can be drawn. For our system, the continuous time averaged model can be obtained by replacing the switched signal $u(t)$ by its duty cycle, given by:

$$d(t) = \frac{1}{2}\left(\frac{v_{con}(t)}{V_u - V_l} + 1\right) \tag{10}$$

The switched vector of state variables is also substituted by its average $\bar{\mathbf{x}}$. In doing so, we obtain the following averaged model for the system:

$$\dot{\bar{\mathbf{x}}} = \mathbf{A}\bar{\mathbf{x}} + (\mathbf{B}_1(t) - \mathbf{B}_2(t))\frac{1}{2}\left(\frac{\bar{v}_{con}(t)}{V_u - V_l} + 1\right) + \mathbf{B}_2(t) \tag{11}$$

Matrix operations in Eq. (11) gives

$$\frac{d}{dt}\begin{pmatrix} \bar{v}_C \\ \bar{i}_L \\ \bar{v}_{con} \end{pmatrix} = \begin{pmatrix} -\frac{1}{RC} & \frac{1}{C} & 0 \\ -\frac{1}{L} & 0 & \frac{1}{L}\frac{V_{\text{in}}}{V_u - V_l} \\ -\frac{k_v}{\tau_v} & 0 & -\frac{1}{\tau_v} \end{pmatrix}\begin{pmatrix} \bar{v}_C \\ \bar{i}_L \\ \bar{v}_{con} \end{pmatrix} + \begin{pmatrix} 0 \\ 0 \\ \frac{k_v}{\tau_v} v_{\text{ref}} \end{pmatrix} \tag{12}$$

which is a linear time-varying model.

2.5. Stability analysis using the small signal averaged model

In order to get the small signal transfer function, the reference signal is considered constant and the model is perturbed to get the small signal incremental model. In this way, the small signal control-to-output loop gain is:

$$G(s) := \frac{\tilde{v}_C(s)}{\tilde{v}_{\text{ref}}(s)} = \frac{k_v V_{\text{in}} \omega_0^2}{(V_u - V_l)(1 + s\tau_v)(s^2 + 2\zeta\omega_0 s + \omega_0^2)} \tag{13}$$

where $\tilde{x}$ stands for small variation near the operating point, $\zeta = (2R\sqrt{C/L})^{-1}$ and $\omega_0 = 1/\sqrt{LC}$. The phase margin ϕ_m can be used, as a test on $G(s)$, to determine the stability of the closed loop system $H(s) := G(s)/(1 + G(s))$. The crossover frequency ω_c is defined as the frequency where the modulus $|G(j\omega_c)| = 1$. The phase margin ϕ_m is determined from the phase of $G(s)$ at ω_c , as follows:

$$\phi_m = \pi + \angle G(j\omega_c) \tag{14}$$

If there is exactly one crossover frequency, and if $G(s)$ contains no RHP poles, then the closed loop system $G(s)/(1+G(s))$ contains no RHP poles whenever the phase margin ϕ_m is positive.

2.6. Parameter selection

Nominal DC input values for DC to AC inverters can be 12 V, 24 V, 36 V, 48 V, 110 V, 125 V, and 250 V. In this paper an input voltage $V_{\text{in}} = 36$ is considered. Other important output specifications to consider when designing a DC to AC inverter include maximum voltage, maximum steady state current, maximum power, and frequency range. The output reference voltage peak-to peak or equivalently its RMS value is set in function of the application. The steady state load current and maximum power is given by the load R. The filter inductor value L is chosen such that the voltage drop across the inductor is less than 1% of the inverter output voltage, i.e.

$$\omega_r L < 1\% R \tag{15}$$

where $I_{R,m}$ is the maximum RMS load current and ω_r is the reference frequency. The frequency range is selected by appropriately by choosing the output capacitor which is chosen so that the system have a certain resonance frequency ω_0:

$$C = \frac{1}{\omega_o^2 L} \tag{16}$$

Finally, the switching frequency is selected in such a way that $10\omega_0 < \omega_s := 2\pi f_s$. By taking into account these considerations, the value of the circuit parameters that will be used in this paper are shown in Table I. The design parameters k_v, τ are selected in order to get a desired phase margin.

Table I. Parameter values used in numerical simulations.

Parameter	Value
V_{in}	36 V
L	200 μH
C	10μF
R	[20 Ω, 5 Ω]
$f_r = \omega_r/2\pi$	50 Hz
f_s	50 kHz
V_l	-1
V_u	1 V
V_r	28 V
k_v	$\in (0.4, 1.4)$
τ_v	$\in (0.1\ \mu s, 10$ ms)

By considering these parameters, different plots are performed to reveal the most important aspects concerning the stability and performances of the system. The phase margin ϕ_m, the gain margin g_m and the crossover frequency ω_c for two different values of the load resistance are plotted in terms of the design parameters τ_v and k_v in Fig. 2 and Fig. 3 respectively. The root locus of the closed loop system by varying the parameters k_v and τ_v are shown in Fig. 4. Based on the figures obtained from the linearized time invariant averaged model we can cite the following statements concerning the stability and dynamical performances of the system:

- it is convenient to avoid using a value of τ_v near $\tau_{v,min}$ as the phase and the gain margins in this zone are at their minimum value and there is a strong risk of instability in this case.
- for values of $\tau_v >> \tau_{v,min}$, the system presents a phase margin ϕ_m and a gain margin g_m much higher than that for values of $\tau_v << \tau_{v,min}$.
- the phase margin decreases when the load resistance R increases.
- the crossover frequency increases when k_v increases and it decreases when τ_v decreases.
- for lower values of load resistance R, the system root locus are moved to the left side making the system more stable (Fig. 4). The gain and the phase margins are also better for low values of R.
- for values of τ_v very far from $\tau_{v,min}$, the system is stable for all gains $k_v \in (0, 1)$.

It will be shown later that this last statement is only true if dealing with slow scale stability. In particular in this zone the system may present subharmonic oscillations if the parameter k_v is increased.

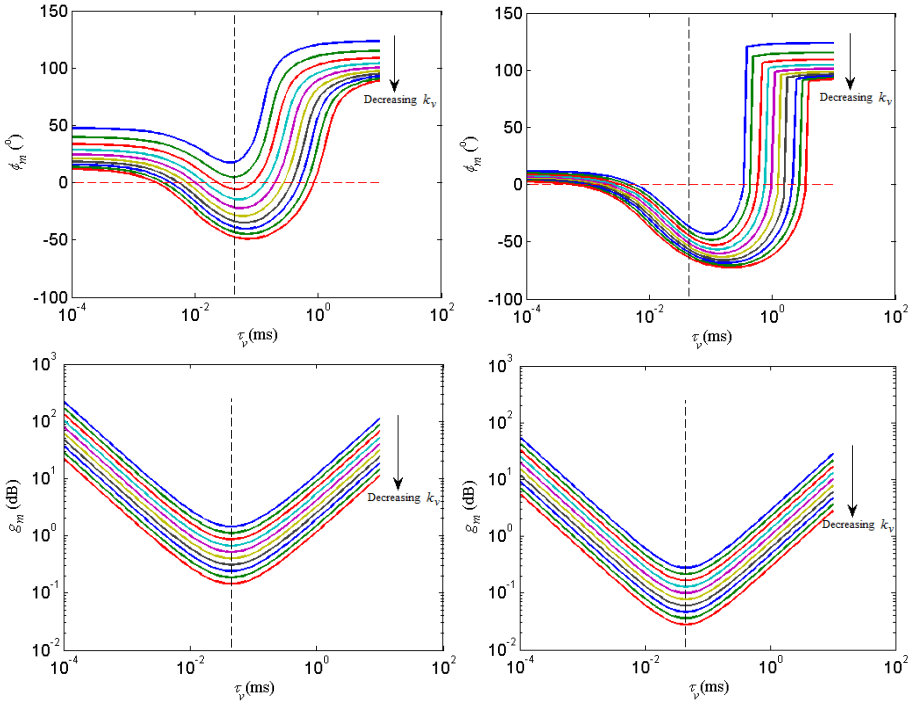

Figure 2. The phase margin ϕ_m and the gain margin g_m vs. the design parameters τ_v and k_v. Left: $R = 5\ \Omega$. Right: $R = 20\ \Omega$.

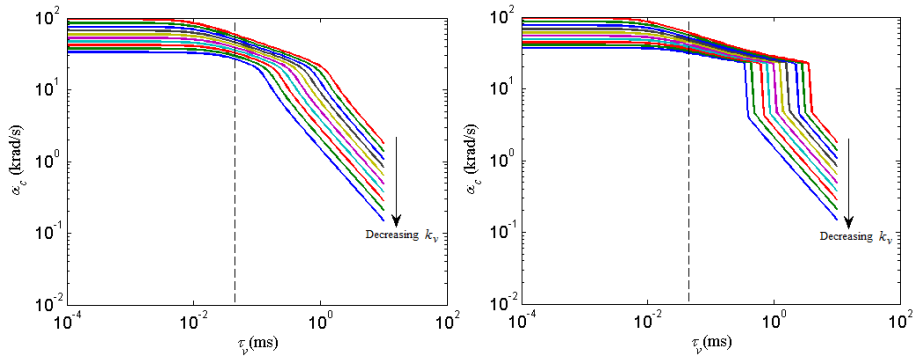

Figure 3. The crossover frequency ω_c in terms the design parameters τ_v and k_v. Left: $R = 5\ \Omega$. Right: $R = 20\ \Omega$.

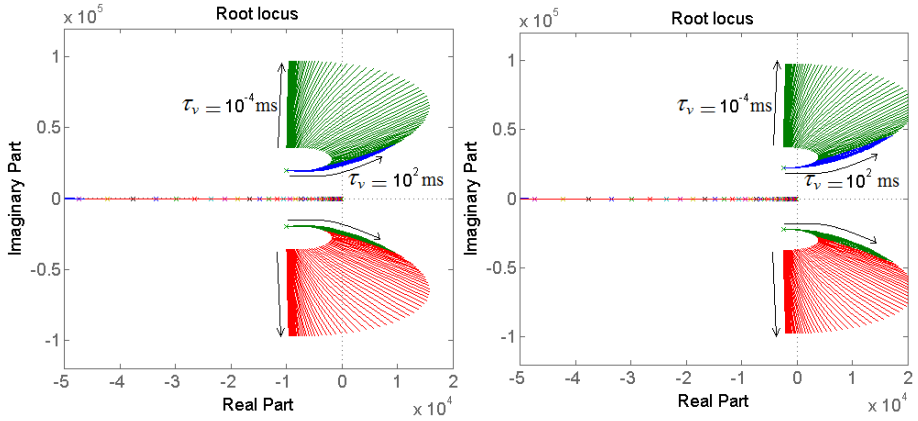

Figure 4. The root locus of the closed loop system by varying the design parameters τ_v and k_v. Left: $R = 5\ \Omega$. Right: $R = 20\ \Omega$. Arrows indicates the motion of the roots when k_v is increased.

2.7. Stability boundary from the averaged model

The characteristic polynomial of the linearized averaged system is independent on the operating point and it can be written as follows:

$$p_3(\lambda) = \lambda^3 + a_2\lambda^2 + a_1\lambda + a_0 \tag{17}$$

where

$$a_2 = \frac{1 + \omega_v\tau_C}{\tau_C},\ a_1 = \omega_0^2(1 + \tau_L\omega_v),\ a_0 = \omega_v\omega_0^2\left(1 + k_v\frac{V_{\rm in}}{V_{\rm m}}\right) \tag{18}$$

where $V_{\rm m} = V_u - V_l$ is the amplitude of the ramp modulator, $\tau_L = L/R$ and $\tau_C = RC$. By applying the Routh-Hurwitz criterion we obtain the following critical value of k_v in terms of τ_v:

$$k_{v,cri} = \frac{V_{\rm m}}{V_{\rm in}}\frac{\tau_v^2 + \tau_L\tau_v + \omega_0^{-2}}{\tau_v\tau_C} \tag{19}$$

which indicates that $k_{v,cri}$ is a unimodal function of τ_v and it presents a minimum at $\tau_{v,min} = \omega_0^{-1}$. The value of $k_{v,cri}$ at $\tau_{v,min}$ is:

$$k_{v,min} = \frac{V_{\rm m}}{V_{\rm in}} \omega_0 \tau_L (2 + \omega_0 \tau_C^{-1}) \tag{20}$$

Figure 5 shows the stability boundary in the (τ_v, k_v) plane for different values of load resistance R in the range shown in Table I. In order to make the figure clear the boundary is plotted in a suitable logarithmic scale. It is worth noting here that this is an approximated approach and some of the nonlinear phenomena like period-doubling bifurcation is not reflected in Fig. 5. Later we will show by using the exact switched model that the system can present subharmonic oscillations at the switching period. This phenomenon will also be obtained by a discrete time model.

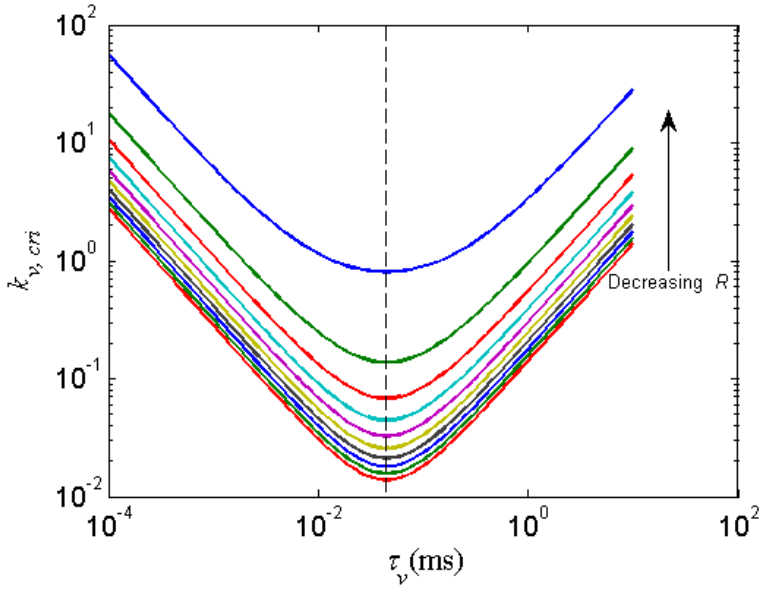

Figure 5. Stability boundary in the (τ_v, k_v) plane for different values of load resistance R. The value of $\tau_{v,min} = \omega_0^{-1}$ is indicated by a vertical dashed line.

3. Possible Nonlinear Phenomena of the System from the Switched Model

The main steady-state periodic waveforms of the system are depicted in Fig. 6. The system trajectory evolves to a two-dimensional torus characterized by two periods that are the switching period and the reference sinusoidal voltage period. In order to make the waveforms more clear and to uncover some possible instability that the system may undergo, the state variables are sampled at the switching period T_s. This is equivalent to taking a first order

Poincaré section. The result is shown in Fig. 7-a. The first order Poincaré section of the steady-state trajectory of the system is an invariant closed curve indicating that the attractor in the continuous time domain is effectively a torus. If the ratio between the reference signal period and the switching period is a rational number, as it is the case in this paper, the attractor is periodic (resonant torus). Its Poincaré section is a set of points on a closed curve. Figure 7-b depicts the Bode plot showing the gain margin, the phase margin and the crossover frequency. From the figure we can see that the system presents a phase margin $\phi_m = 86.4^o$ at a frequency $\omega_c \approx 2.5$ krad/s which acceptable for practical uses.

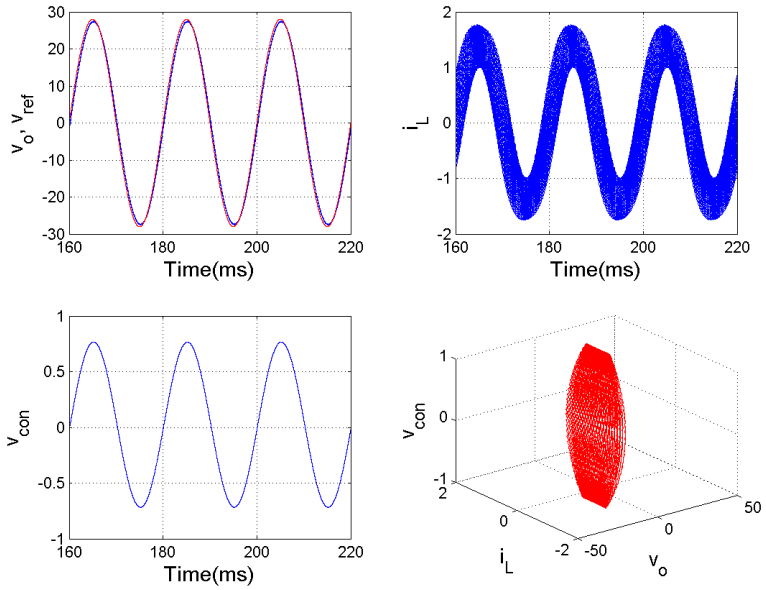

Figure 6. Waveforms of a DC-AC buck inverter showing normal periodic behavior. $k_v = 1.3$, $\tau_v = 10ms$, $R = 5\ \Omega$. Other parameters are given in Table I.

It is important to note that the maximum reference voltage V_r must be smaller than the input voltage V_{in} for the system to operate in normal operation (as it corresponds to a buck converter). In order to achieve output voltage tracking, the reference signal τ_v and k_v should be adjusted appropriately in order to guarantee stable behavior for the complete dynamic range of the reference voltage. Improperly adjusted values can give rise to different kinds of instabilities as it will be shown later. In a practical design procedure, the aim is to decrease the static error at the output and to maintain stable behavior. Note for example, from Fig. 6, that good tracking exists between the reference signal and the output voltage. In order to achieve a small quasi-static error, the gain k_v (time constant τ_v) should be taken in such a way that the crossover frequency is much smaller than the switching frequency.

Under parameter changes, the desired periodic solution could loose stability resulting in a behavior of the system with different dynamic characteristics to that of Fig. 6. Torus bifurcations at the switching period may occur. Both period-doubling and Neimark-Sacker bifurcations are possible. For instance, a stable periodic solution can undergo a Neimark-Sacker bifurcation at the switching period (Fig. 8). After this bifurcation takes place another

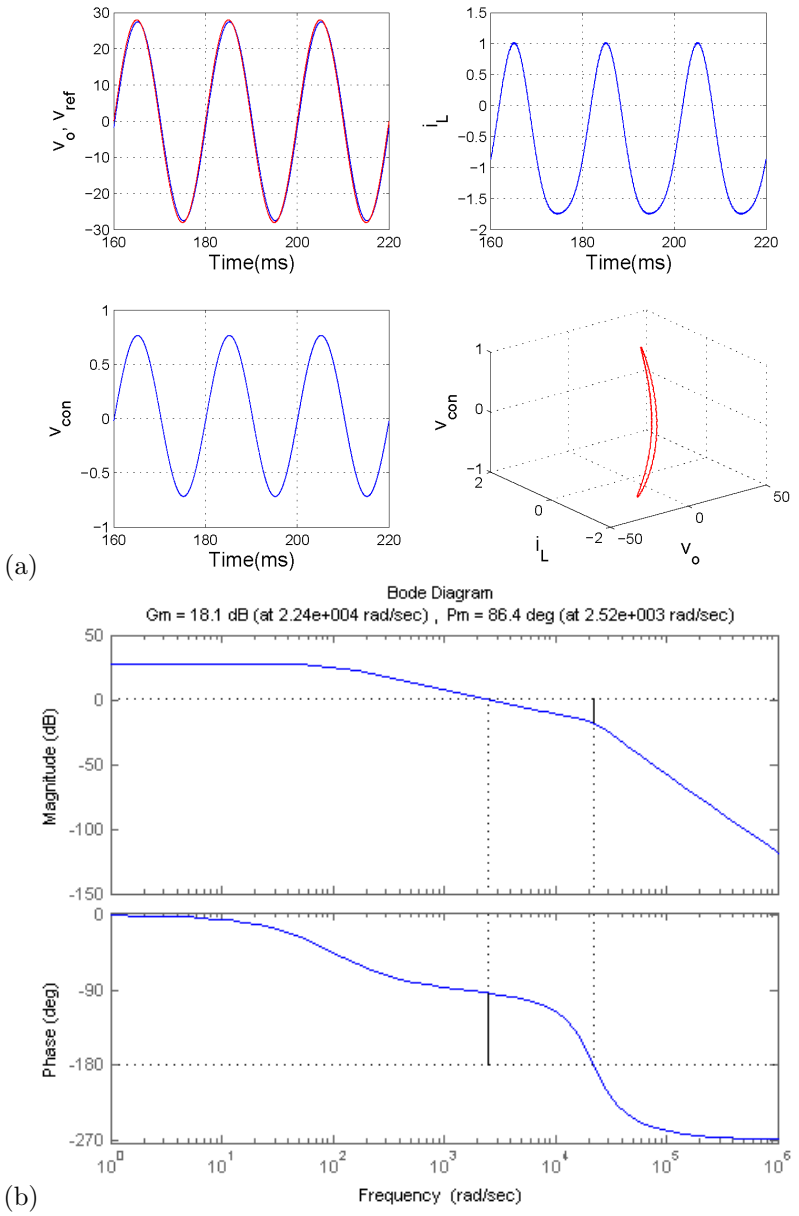

(a)

(b)

Figure 7. Time domain T_s-sampled waveforms and Bode plot showing the gain margin, the phase margin and the crossover frequency. $\tau_v = 10\ ms$, $R = 5\ \Omega$. Other parameters are given in Table I.

frequency f_0 ($f_r < f_o < f_s$) appears in the dynamics of the system [21], [22]. Simulation results show that this instability can be detected by using a time-varying averaged model. However the results obtained based on this model are less accurate than those obtained from

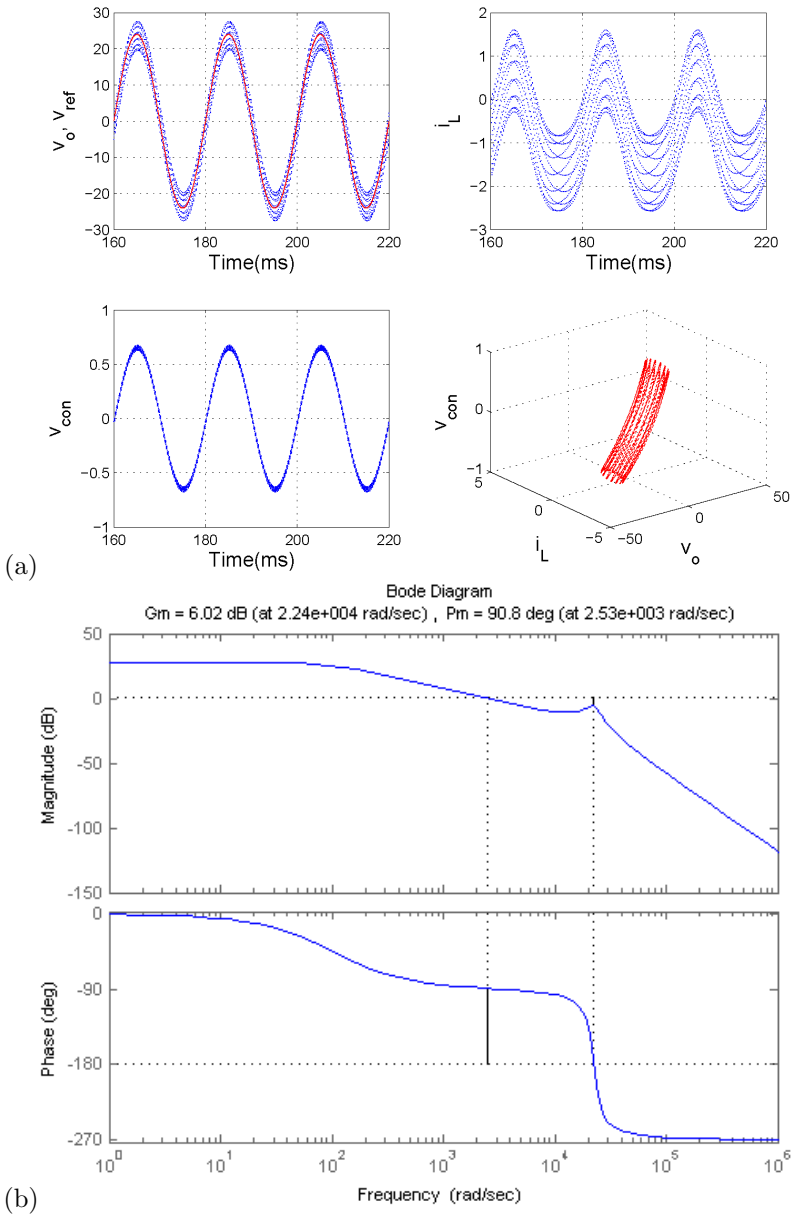

Figure 8. (a) T_s-sampled waveforms showing Quasiperiodic behavior after a Neimark-Sacker bifurcation occurs. (b) Bode plot showing the gain margin, the phase margin and the crossover frequency. $k_v = 1.39$, $\tau_v = 10\ ms$, $R = 20\ \Omega$. Other parameters are from Table I

the switched model. From Fig. 8-b, we can conclude that the system presents an acceptable phase and gain margin. However from the numerical simulation of Fig. 8-a, it is clear that the

system is unstable. This is one of the shortcomings of the averaged model in describing the dynamics of switched circuits. We will show later that, instead, the discrete-time model yields highly accurate results concerning the dynamics of the system.

Another well known bifurcation phenomenon in power electronics circuits is period-doubling bifurcation at the switching period. In an DC-AC inverter, this bifurcation is also possible if some suitable parameters are varied. Figure 9-a depicts the waveforms of the system showing this period-doubling phenomenon. It is clear from this figure that this phenomenon results in subharmonic oscillations near the minimum and maximum values of the first order error amplifier output and the inductor current waveforms. Usually this period-doubling phenomenon usually culminates in a chaotic behavior after successive torus doubling [23]. Figure 9-b depicts the Bode plot showing the gain margin, the phase margin and the crossover frequency. From this figure we can see that the system presents a poor phase margin $\phi_m = 14.4^o$ at a frequency $\omega_c \approx 83$ krad/s.

It should be noted that the period-doubling instability at the switching period cannot be detected by using the averaged model. The detection of this instability requires the derivation of a discrete-time model. In the next section we will give a systematic procedure to obtain this model for the voltage-mode controlled DC-AC inverter of Fig. 1. This model is shown to be able to predict most of the dynamical behaviors that can be predicted by the exact switched model.

4. Description of the System Dynamics by a Discrete-time Model

Accurate discrete-time models are derived from regular sampling of the state variables of the continuous-time dynamics [25], [26]. This model does not assume the approximations taken in the averaged modeling approach such as small ripple and high switching frequency and it is shown to be an accurate model in predicting the different kinds of instabilities of power electronics systems.

It is worth noting here that the discrete-time model is not obtained by simple discretization of the continuous model. It is obtained by using the exact solutions of the switching system during each sub-interval. Being characterized by two different forcing periods, two kinds of discrete-time modeling for the system can be obtained. If we are concerned with the dynamics of the system within the switching cycle, the first order discrete-time model can be defined from the current switching cycle to the next one. This is the mapping that relates the state variables from the beginning to the end of a switching cycle. If the dynamics of the system during a reference cycle is pursued, then the second order discrete-time model is considered [9], [24]. In this paper, we will obtain the first order discrete-time model. The system configuration during each switching sub-interval is linear and time-varying as it is mentioned earlier. During phase 1 the trajectory of the system, starting from the initial condition $\mathbf{x}_n$, is expressed by:

$$\mathbf{x}(t) = e^{\mathbf{A}(t-nT_s)}\mathbf{x}_n + \int_{nT_s}^{nT_s+t} e^{\mathbf{A}\tau}\mathbf{B}_1(\tau)d\tau \tag{21}$$

At time instant d_nT the system switches from phase 1 to phase 2. This instant can be determined from the equation resulting from the crossing of the ramp signal $v_{\text{ramp}}(t)$ with the control voltage $v_{con}(t)$. This equation is given by:

$$\sigma(\mathbf{x}, d_n) := v_{con}(d_nT_s) - V_l - (V_u - V_l)d_n = 0 \tag{22}$$

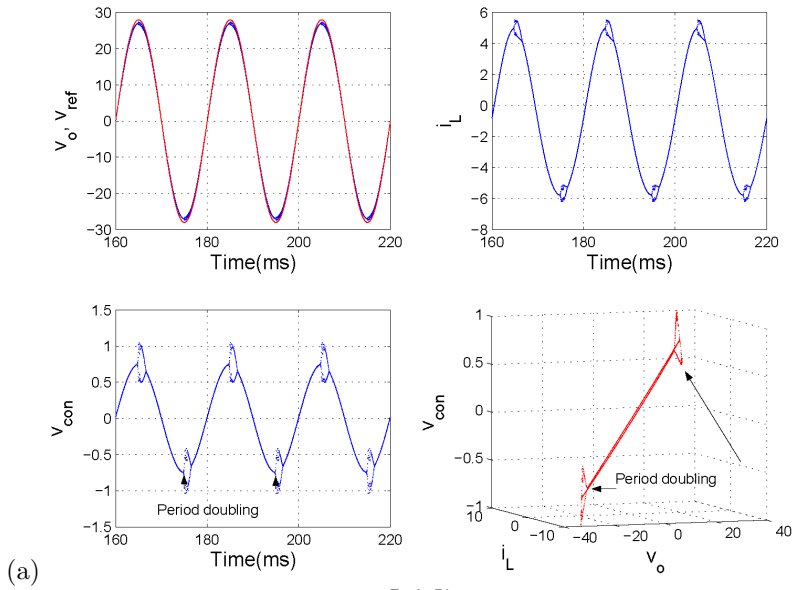

(a)

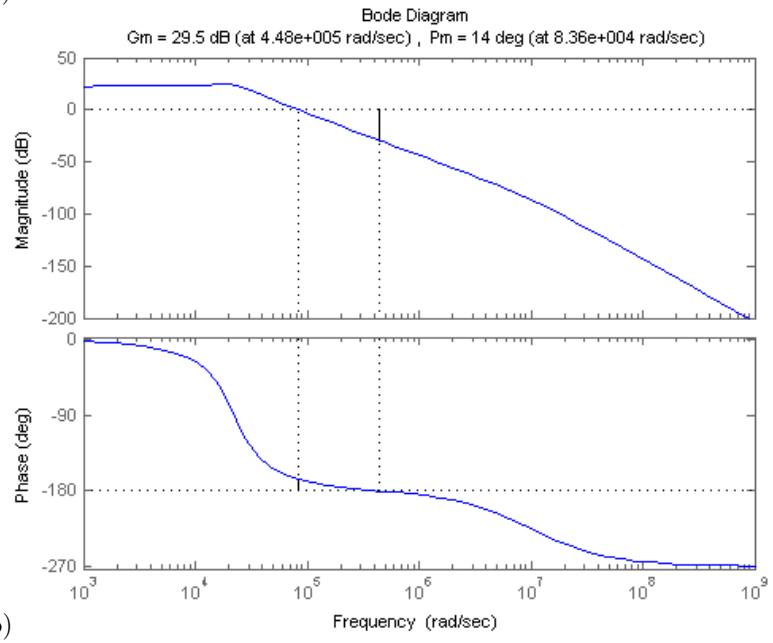

(b)

Figure 9. (a) T_s-sampled waveforms of a DC-AC buck inverter showing subharmonic oscillations after a period-doubling bifurcation occurs. (b) Bode plot showing the gain margin, the phase margin and the crossover frequency. $k_v = 0.745$, $\tau_v = 0.1\ \mu s$, $R = 5\ \Omega$. Other parameters are from Table I.

At the instant $(n+1)T$ the system switches to phase 1 again. The state of the system at time

instant $(n+1)T_s$ is given by:

$$\mathbf{x}_{n+1} = e^{\mathbf{A}T_s}\mathbf{x}_n + e^{\mathbf{A}(1-d_n)T_s}\int_{nT_s}^{(n+d_n)T_s} e^{\mathbf{A}\tau}\mathbf{B}_1(\tau)d\tau + \int_{(n+d_n)T_s}^{(n+1)T_s} e^{\mathbf{A}\tau}\mathbf{B}_2(\tau)d\tau \tag{23}$$

It is worth noting here that (22) is a transcendental equation and that a root finding algorithm must be applied in order to obtain the duty cycles for each switching period. In order to simplify the expression of the first order map, let us write it in the following form:

$$\mathbf{x}_{n+1} := \mathbf{P}(\mathbf{x}_n, n) = \mathbf{\Phi}\mathbf{x}_n + \mathbf{\Phi}_2\mathbf{\Psi}_1(n) + \mathbf{\Psi}_2(n) \tag{24}$$

where

$$\begin{array}{l} \mathbf{\Phi} = e^{\mathbf{A}T} \\ \mathbf{\Phi}_1 = e^{\mathbf{A}d_nT}, \quad \mathbf{\Phi}_2 = e^{\mathbf{A}(T-d_nT)}, \\ \mathbf{\Psi}_1(n) = \int_{nT}^{(n+d_n)T} \mathbf{\Phi}_1\mathbf{B}_1(\tau)d\tau, \\ \mathbf{\Psi}_2(n) = \int_{(n+d_n)T}^{(n+1)T} \mathbf{\Phi}_2\mathbf{B}_2(\tau)d\tau \end{array} \tag{25}$$

Note that the vectors $\mathbf{\Psi}_k(n)$ are time-dependent, making the first order Poincaré map time-varying. Once the matrix $\mathbf{\Phi}_k$ is obtained, an expression for matrix $\mathbf{\Psi}_k(n)$ can be found from Eq. (25). The exponential matrix $\mathbf{\Phi}_k$ can be obtained by using the Cayley-Hamilton theorem and the Putzer method [27]. For simplicity of integration of the system equations during each phase, the vectors $\mathbf{B}_1(t)$ and $\mathbf{B}_2(t)$ can be written as the sum of a constant term $\mathbf{B}_a$ and a T_r-periodic time-varying term $\mathbf{B}_b\sin(\omega_r t)$:

$$\mathbf{B}_1(t) = \mathbf{B}_a^+ + \mathbf{B}_b\sin(\omega_r t), \;\; \mathbf{B}_2(t) = \mathbf{B}_a^- + \mathbf{B}_b\sin(\omega_r t) \tag{26}$$

where

$$\mathbf{B}_a^{\pm} = \begin{pmatrix} 0 \\ \pm\dfrac{V_{\text{in}}}{L} \\ 0 \end{pmatrix} \text{ and } \mathbf{B}_b = \begin{pmatrix} 0 \\ 0 \\ \dfrac{k_v}{\tau_v}V_r \end{pmatrix} \tag{27}$$

By computing the integral term in (21), $\mathbf{\Psi}_1(n)$ can be expressed as:

$$\begin{aligned} \mathbf{\Psi}_1(n) = (\mathbf{A}^2 + \omega_r^2\mathbf{I})^{-1}[&\omega_r\mathbf{\Phi}_1\mathbf{B}_b\cos(n\omega_r T_s) + \mathbf{\Phi}_1\mathbf{A}\mathbf{B}_b\sin(n\omega_r T_s) - \omega_r\mathbf{B}_b\cos((n+d_n)\omega_r Ts) \\ &-\mathbf{A}\mathbf{B}_b\sin((n+d_n)\omega_r T_s)] + \mathbf{A}^{-1}(\mathbf{\Phi}_1 - \mathbf{I})\mathbf{B}_a^+ \end{aligned} \tag{28}$$

where it has been considered that

$$\int_0^t e^{\mathbf{A}\tau}\sin(\omega_r\tau)d\tau = (\mathbf{A}^2+\omega_r^2\mathbf{I})^{-1}[\omega_r e^{\mathbf{A}t}\cos(\omega_r t)+e^{\mathbf{A}t}\mathbf{A}\sin(\omega_r t)-\mathbf{I}\omega_r\cos(\omega_r t)-\mathbf{A}\sin(\omega_r t)] \tag{29}$$

and that

$$\int_0^t e^{\mathbf{A}\tau}d\tau = \mathbf{A}^{-1}(e^{\mathbf{A}t} - \mathbf{I}) \tag{30}$$

where it has been assumed without loss of generality that $\mathbf{A}$ is not singular. Note that if a PI controller for the output voltage is used instead of a low pass filter, this matrix is actually singular and expression (30) is not valid but the integral is still well defined. The vector $\mathbf{\Psi}_2(n)$ can be obtained in the same way by substituting $\mathbf{\Phi}_1$ by $\mathbf{\Phi}_2$ and $\mathbf{B}_b^+$ by $\mathbf{B}_b^-$ in (28). Note that different expressions for $\mathbf{\Psi}_k$ $(k=1,2)$ would have been obtained if the reference voltage would

have been considered constant (quasi-static approximation). Note also that the function $\mathbf{\Psi}_k$ corresponding to a constant reference voltage can be obtained by forcing $\omega_r = 0$ in Eq. (28). Once both $\mathbf{\Phi}_k$ and $\mathbf{\Psi}_k(n)$ are obtained and combined with Eq. (22), the expression of $\mathbf{P}$, the first order map is obtained from Eq. (24). $\mathbf{P}$ is the mapping that relates the vector of the state variables $\mathbf{x}_n$ at the beginning of the switching cycle to $\mathbf{x}_{n+1}$, those at the end of the same cycle. Note that it is a non-linear map in the state variables and periodically time-varying in the discrete-time domain. This non-linear time-varying map has a periodic orbit (not a fixed point) as a nominal operating regime.

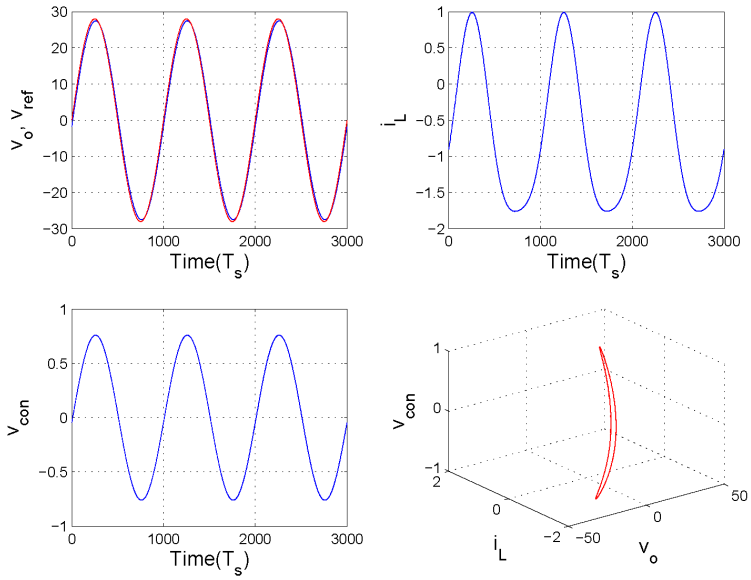

Figure 10. Waveforms of a DC-AC buck inverter from the discrete-time model showing normal periodic stable behavior. $k_v = 1.3$, $\tau = 10\ ms$, $R = 20\ \Omega$. Other parameters are form Table I.

Numerical simulations are carried out using this map in a MATLAB code and an iterating procedure to generate the discrete-time waveforms. The results are obtained by using the same parameter values than their corresponding time domain simulations from the switched model. Simulations corresponding to these cases are shown in Fig. 10, Fig. 11 and Fig. 12. Figure 10 corresponds to the stable operation of the system while Fig. 11 and Fig. 12 correspond to the switching frequency instability in the form of Neimark-Sacker and period-doubling bifurcation, respectively. These figures result from the numerical simulation using the developed discrete-time model at the same tested circuit parameters of Fig. 6, Fig. 8 and Fig. 9, respectively. As it can be observed there is a perfect agreement between the results obtained from the numerically integrated switched model and the proposed analytical discrete-time model. However, the results obtained from the proposed model are much faster than those obtained by using the switched model as it is always more easy to iterate a recurrence equation than to numerically integrate a differential equation.

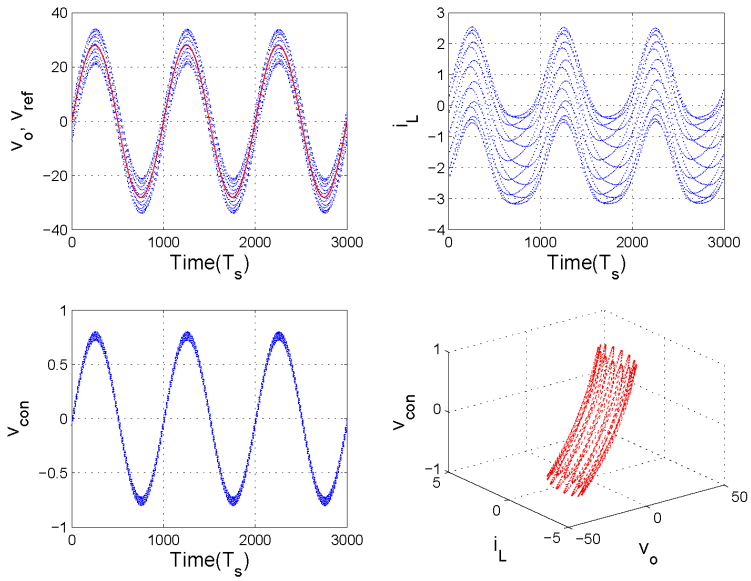

Figure 11. Waveforms of a DC-AC buck inverter from the discrete-time model showing Neimark-Sacker bifurcation at the switching period. $k_v = 1.39$, $\tau_v = 10\ ms$, $R = 20\ \Omega$. Other parameters are form Table I.

5. Stability Boundary from the Discrete Time Model

In this section, the useful region in the parameter space of the DC-AC buck-based inverter will be obtained. Practical issues clarify that inverter design must assure stability over the load range (from full load to light load). Therefore, the load R is chosen as the main investigated parameter. Moreover, the gain of the voltage corrector k_v and its time constant τ_v are the selected feedback parameters that control the inverter performance. The gain should be high enough to guarantee the inverter output regulation, while avoiding instability. Also, the time constant should be adjusted for acceptable system response. Therefore, the system stability will be tested based on the parametric space R, k_v and τ_v. All other parameters are considered constant as shown in Table I. To obtain stability borders, the selected parameters have been varied, and the system is tested for stability. A three-dimensional (3D) stability map has been obtained to show the stability boundary based on the parametric sweep. The values of τ_v and R have been varied in a suitable two-dimensional (2D) grid and for each point in this grid, the value of k_v is increased to force bifurcation. The critical value is recorded and the process is repeated for the complete set of points belonging to the grid as shown in Fig. 13. The results are obtained from both the switched model and the discrete-time model. Stability regions are under the curves. From this figure, it is clear that the system becomes more prone to instability as the operation moves into light load, high DC gain and high time constant. Also, Fig. 13 (down) shows the stability boundary in the two-dimensional design parameter space. The same results can be noticed, but with more accurate border. It is worth to note that the results obtained from our model match well with those obtained from the exact switched

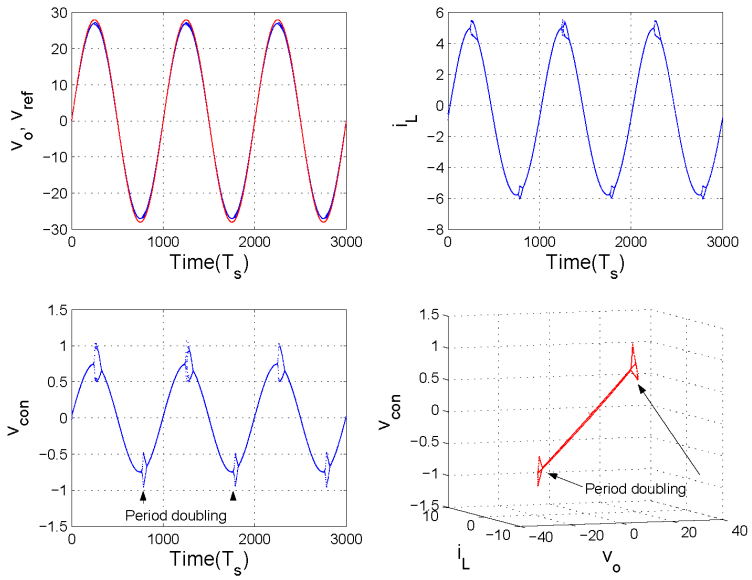

Figure 12. waveforms of a DC-AC buck inverter from the discrete-time model showing period-doubling at the switching period, $k_v = 0.745$, $\tau_v = 0.1\ \mu s$, $R = 5\ \Omega$. Other parameters are form Table I.

model. However the simulations using discrete-time model are much faster, which can provide a way of designing for stable operation using these 3D or 2D boundaries in the design parameter space. For instance, for the simulations of Fig. 8 and Fig. 11, the ratio of simulation time was 15:1, which results in a reduction of computational load of 1500:1 for the complete design space exploration (Fig. 13). Based on the figures obtained from discrete time model we can cite the following conclusions:

- for values $\tau_v >> \tau_{v,min}$, the results obtained from the analytical expressions based on the averaged model (Fig. 5) are in good concordance with those obtained from the switched model and the discrete time model (Fig. 13). This concordance can be explained as follows: the control voltage v_{con} is almost ripple free at the switching period due to the low pass filtering. The averaged model is a good approximation of the exact switched model in this case.
- for values $\tau_v << \tau_{v,min}$ and for low values of R (in our case $R = 5\ \Omega$), the system can present subharmonic oscillations not detected by the averaged model. This disagreement can be explained by the fact the control voltage v_{con} contains ripple at the switching period because the corner frequency of the low pass filter is relatively high. The averaged model gives erroneous results concerning the stability of the system in this case.

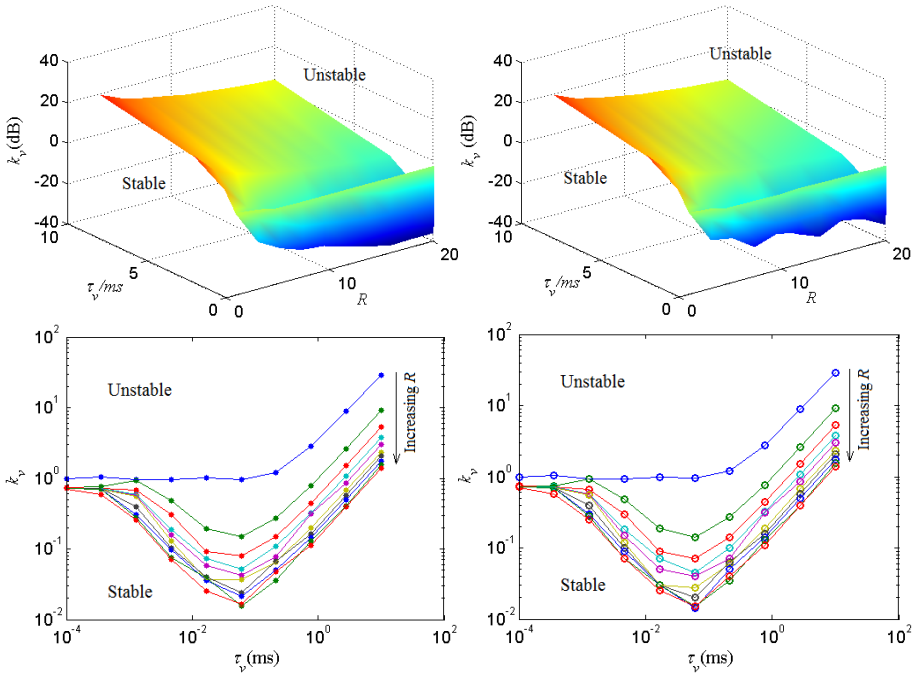

Figure 13. Stability boundaries in 2D and 3D design parameter spaces. Left: Discrete time model. Right: Switched model.

Conclusion

Different bifurcation phenomena are detected and studied for a full bridge DC-AC buck inverter under low-pass compensated voltage-mode control and PWM modulation fixed frequency strategy. Instabilities at the switching period can occur. An averaged model is derived and it was used to obtain some analytical expressions concerning the dynamical behavior of the system. Although some phenomena, like Neimark Sacker bifurcation at the switching period, can be detected by using an averaged approach, other instabilities require a discrete-time model to be detected. The simulation results presented throughout the paper show that oscillations at switching period can occur if the system parameters of the system are not well designed. This clearly requires an accurate model to get a deep understanding of the dynamic characteristics of the system at the switching scale. Such model was derived and it was shown to be able to accurately predict the different instability phenomena that can occur at the switching period. The model was derived without making traditional assumptions like the quasi-static approximation. From the simulation of the circuit, it can be claimed that all parameters influence the dynamics at the switching period. To obtain a stable periodic behavior, these parameters should be appropriately adjusted. Stability of the system at the switching period can be ensured by choosing appropriate values of the ramp slope, static gain k_v and time constant τ_v according to the value of the maximum conversion ratio V_r/V_{in} and inductance L. Future works will deal with the application of the discrete-time model to other more complex

time-varying power electronics circuits such as multi-phase and multi-level inverters.

Acknowledgments

The authors would like to thank the anonymous reviewers for their valuable comments and suggestions that helped to improve an original version of the paper. This work was partially supported by Agencia Española de Cooperación Internacional (AECI) under grant A/012533/07 and the Spanish Ministerio de Educación e Innovación under grant TEC-2007-67988-C02-02.

REFERENCES

1. M. Zhu, F. L. Luo, "Transient analysis of multi-state dc-dc converters using system energy characteristics", *International Journal of Circuit Theory and Applications*, vol. 36, Issue 3, May 2008, pp. 327-344.
2. C. K. Tse "Chaos from a buck switching regulator operating in discontinuous mode", *International Journal of Circuit Theory and Applications*. vol. 22, no. 4, pp. 263-278, 1994.
3. William C. Y. Chan, C. K. Tse, "Bifurcations in current-programmed DC/DC buck switching regulators - conjecturing a universal bifurcation path" *International Journal of Circuit Theory and Applications*, vol. 26, Issue 2, March/April 1998, Pages: 127-145
4. C. K. Tse "Chaos from a buck switching regulator operating in discontinuous mode", *International Journal of Circuit Theory and Applications*. vol. 22, no. 4, pp. 263-278, 1994.
5. William C. Y. Chan, C. K. Tse, "Bifurcations in current-programmed DC/DC buck switching regulators - conjecturing a universal bifurcation path" *International Journal of Circuit Theory and Applications*, vol. 26, Issue 2, March/April 1998, Pages: 127-145
6. X. Wu, C. K. Tse, S. C. Wong and J. Lu, "Fast-scale bifurcation in single-stage PFC power supplies operating with DCM boost stage and CCM forward stage," *International Journal of Circuit Theory and Applications*, vol. 34, no. 3, pp. 341-355, 2006.
7. C. K. Tse and W. C. Y. Chan, "Chaos from a Current-Programmed Cuk Converter," *International Journal of Circuit Theory and Applications*, vol. 23, no. 3, pp. 217-225, May-June 1995.
8. M. Orabi, T. Ninomiyam, "Nonlinear Dynamics of Power-Factor-Correction Converter", *IEEE Transactions on Industrial Electronics*, vol. 50, no. 6, pp. 1116-1125, 2003.
9. S. K. Mazumder, M. Alfayyoumi, A. H. Nayfeh, and D. Borojevic, "An Investigation Into Fast- and Slow-Scale Instabilities of a Single Phase Bidirectional Boost Converter", *IEEE Transactions on Power Electronic*, vol. 18, no. 4, pp. 1063–1069, 2003.
10. S. K. Mazumder, M. Alfayyoumi, A. H. Nayfeh, and D. Borojevic, "A Novel Approach to the Stability Analysis of Boost Power-Factor-Correction Circuits", *IEEE Power Electronic Specialist Conferences, PESC'01*, British Culombia, Canada, pp. 1719-1724, 2001.
11. A. El Aroudi, M. Orabi and Luis-Martínez-Salamero, "A Representative Discrete-time Model for Uncovering Slow and Fast Scale Instabilities in Boost Power Factor Correction AC-DC Pre-regulators", in *International Journal of Bifurcations and Chaos* IJBC, vol. 18, No. 10, pp. 3073-3092, 2008.
12. J. Zou, X. Ma, C. K. Tse and D. Dai, "Fast-scale bifurcation in power-factor-correction buck-boost converters and effects of incompatible periodicities", *International Journal of Circuit Theory and Applications*, 2006; vol. 34, no. 3, pp. 251-264.
13. B. Basak and S. Parui., "Incompleteness of bifurcation diagram in predicting the behaviour of Čuk converter in discontinuous conduction mode", *International Journal of Circuit Theory and Applications*, vol. 36, Issue 4, June 2008, pp. 387-396.
14. Xiaoqun Wu, Chi K. Tse, Siu Chung Wong, Junan Lu, "Fast-scale bifurcation in single-stage PFC power supplies operating with DCM boost stage and CCM forward stage, *International Journal of Circuit Theory and Applications*, vol.e 34, Issue 3, Date: May/June 2006, pp. 341-355
15. H.-J. Chiu, C.-J. Yao, Y.-K. Lo, "A DC/DC converter topology for renewable energy systems" *International Journal of Circuit Theory and Applications*, vol. 37, Issue 3, April 2009, pp. 485-495
16. B. Zhang, K. Zhou, Y. Wang, D. Wang, "Performance improvement of repetitive controlled PWM inverters: A phase-lead compensation solution", *International Journal of Circuit Theory and Applications*, DOI. 10.1002/cta.572

17. D. Carton, B. Robert, C. Goeldel, "The Use of Method Studying Chaos to Analyse a Current Mode Pulse Width Modulation H-Bridge", *IEEE European Power Electronics Conference*, pp. 3272-3277, Trondheim, Norway, 1997.
18. D. Carton, B. Robert, C. Goeldel, "Study of Chaotic Behaviours of a Current Mode PWM H-Bridge", *Proceeding of the IFAC International Workshop on Motion and Control*, Grenoble, France, 1998.
19. B. Robert, D. Carton, C. Goeldel, "On the modulator influence on Chaotic Behaviours in a PWM Bridge", *Proceeding of the 8th European Conference on Power Electronics and Applications*, EPE'99, Lausane, Switzerland, September, 1999, CD-ROM.
20. B. Robert and C. Robert, "Border Collision Bifurcations in a One Dimentional Piece Wise Smooth Mapfor a PWM Current Programmed H-Bridge Inverter", *International Journal of Control*, 2001.
21. A. El Aroudi and R. Leyva, "Quasi-periodic Route to Chaos in a PWM Voltage Controlled DC-DC Boost Converter", *IEEE Transactions Ciruicts and Systems I*, vol. 48, no. 8, pp. 967-978, 2001.
22. L. Benadero, A. El Aroudi, G. Olivar, E. Toribio and E. Gomez, "Two-Dimensional Bifurcation Diagrams. Background Pattern of Fundamental DC-DC Converters With PWM Control", *International Journal of Bidurcations and Chaos*, vol. 13, no. 2, pp. 427-451, 2003.
23. M. Sekikawa, T. Miyoshi, and N. Inaba, "Successive Torus Doubling", *IEEE Transactions Ciruicts and Systems I*, vol. 48, no. 1, pp. 28-34 2001.
24. A. H. Nayfeh and B. Balachandran, *Applied Nonlinear Dynamics*. John Wiley & Sons, Inc., 1995.
25. G. C. Verghese, M. E. Elbuluk, and J. G. Kasakian, "A General Approach to Sampled-Data Modeling for Power Electronic Circuits," *IEEE Transactions on Power Electronics*, vol. 1, pp. 76–89, 1986.
26. M. di Bernardo and F. Vasca, "Discrete-Time Maps for the Analysis of Bifurcations and Chaos in DC/DC Converters", *IEEE Transactions on Circuits and Systems I*, vol. 47, pp. 130–143, 2000.
27. T. A. Apostol, "Calculus", vol. 2, 2nd edition, John and Wiely Sons, New York, 1988.
28. Damian Giaouris, Somnath Maity, Soumitro Banerjee, Volker Pickert, Bashar Zahawi, "Application of Filippov method for the analysis of subharmonic instability in dc-dc converters", *International Journal of Circuit Theory and Applications*, 2008, DOI: 10.1002/cta.505.
29. William C. Y. Chan, C. K. Tse, "Bifurcations in current-programmed DC/DC buck switching regulators - conjecturing a universal bifurcation path" *International Journal of Circuit Theory and Applications*, vol. 26, Issue 2, March/April 1998, Pages: 127-145
30. C. K. Tse "Chaos from a buck switching regulator operating in discontinuous mode", *International Journal of Circuit Theory and Applications*. vol. 22, no. 4, pp. 263-278, 1994.
31. William C. Y. Chan, C. K. Tse, "Bifurcations in current-programmed DC/DC buck switching regulators - conjecturing a universal bifurcation path" *International Journal of Circuit Theory and Applications*, vol. 26, Issue 2, March/April 1998, Pages: 127-145
32. X. Wu, C. K. Tse, S. C. Wong and J. Lu, "Fast-scale bifurcation in single-stage PFC power supplies operating with DCM boost stage and CCM forward stage," *International Journal of Circuit Theory and Applications*, vol. 34, no. 3, pp. 341-355, 2006.
33. C. K. Tse and W. C. Y. Chan, "Chaos from a Current-Programmed Cuk Converter," *International Journal of Circuit Theory and Applications*, vol. 23, no. 3, pp. 217-225, May-June 1995.
34. H. H. C. Iu, Zhou and C. K. Tse, "Fast-Scale Instability in a Boost PFC Converter Under Average Current Control", *International Journal of Circuits Theory and Applications*, vol. 31, pp. 611-624, 2003.

